Density functional theory for predicting polymeric forces against surface fouling

Xiaofei Xu,[a] Dapeng Cao*[a] and Jianzhong Wu*[b]

Received 26th February 2010, Accepted 23rd April 2010
DOI: 10.1039/c0sm00034e

Polymer-based "non-stick" surfaces have been proposed as the next generation of effective and environmentally-friendly coating materials for protecting implanted biomedical devices and for marine antifouling. However, identification of polymeric systems for universal fouling control is often impeded by the poor knowledge of interactions between biological substances and polymeric substrates in diverse aqueous environments. In this article, we review predictions of the polymer density functional theory (DFT) on the structural and surface properties of polymer brushes and polymer nanocomposites that are potentially useful for antifouling applications. In comparison to alternative theoretical methods, DFT exhibits versatile features that are ideal for investigating various polymer-mediated interactions, self-organization of nanoparticles, and surface-induced phase transitions. It is capable of explicit description of important microscopic details of polymeric systems including the molecular excluded-volume effects, associating interactions, van der Waals attraction, Coulomb forces, and inter- and intra- molecular correlations. The theoretical descriptions of surface forces may provide helpful guidelines in the design and development of polymeric materials for preventing non-specific adsorption of biological substances.

1. Introduction

Antifouling materials are widely used for protection of equipments and devices from non-specific adsorption of biological substances in an aqueous environment.[1,2] For example, ship hull protection from biofouling, *i.e.*, formation of biofilms by microorganisms, is crucial for efficient fleet operation and energy conservation.[3] Biofouling is undesirable because it promotes metal corrosion and increases the hydrodynamic drag and consequently fuel consumption. Similarly, cells and biomacromolecules attached onto an implanted medical device often spoil its performance and lead to host infection.[4] While it is well documented that non-specific adsorption of biological substances can be significantly reduced by surface modification with hydrophilic polymers such as poly (ethylene oxide) (PEO) or poly (ethylene glycol) (PEG),[5] the durability of these polymers

[a]*Division of Molecular and Materials Simulation, Key Lab for Nanomaterials, Ministry of Education, Beijing University of Chemical Technology, Beijing, 100029, P. R. China. E-mail: caodp@mail.buct.edu.cn*
[b]*Department of Chemical and Environmental Engineering, University of California, Riverside, CA, 92521, USA. E-mail: jwu@engr.ucr.edu*

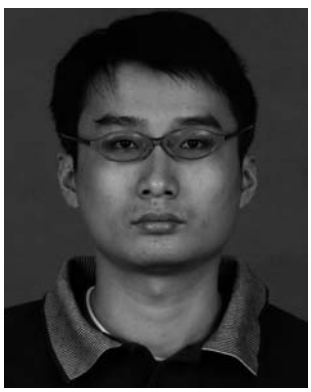

Xiaofei Xu

Xiaofei Xu is a PhD candidate in the College of Chemical Engineering of the Beijing University of Chemical Technology. His main research interests are the microstructure and properties of polymers in complex systems through classical density functional theory. He has published several papers in the Journal of Chemical Physics, Physical Review E, etc.

Dapeng Cao

Dapeng Cao is a professor and associate director of the Lab of Molecular and Materials Simulation at the Beijing University of Chemical Technology (BUCT). He received his PhD from BUCT in 2002, and was a research scientist at Nano-Materials Technology Pte Ltd in Singapore (2002–2003) and a postdoctoral researcher at the University of California at Riverside (2003–2005). His research interests are focused on the design of functional materials by experiments and simulations, including polymer-based functional materials and porous adsorbents such as single-walled carbon nanotube (SWNT), covalent-organic frameworks (COF) and metal- organic frameworks (MOF).

and their long-term performance are often unsatisfactory. It remains a scientific challenge to identify novel antifouling materials that are easy to fabricate and exhibit high antifouling efficiency, minimal ecotoxicity and good durability.[6]

Design and fabrication of novel, non-toxic antifouling materials will be benefited from a detailed knowledge of biofilm formation, in particular, of the physiochemical events in the early stage of microorganism adhesion. The subject has been extensively discussed in the literature and summarized in a number of outstanding reviews.[7–12] Because fouling microorganisms are excessively diversified–more than 99% of all microorganisms on Earth are living in biofilms, it is extremely difficult to establish experimental model systems that provide typical characteristics of biological interactions between a polymeric substrate and microorganisms or biomacromolecules in diverse aqueous environments. However, numerous experimental investigations into the beginning stage of biofouling processes reveal that adhesion of microorganisms onto a substrate is primarily driven by the surface interaction with the extracellular polymeric substances that mainly consist of polysaccharides and proteins.[13,14] Because a similar adhesion behavior occurs for dead and living cells, the initial stages of microbial adhesion are most likely dominated by abiotic processes. As a result, understanding the physiochemical interactions between a polymeric surface and biomacromolecules such as polysaccharides and proteins is essential for design and development of successful antifouling strategies.

Polymer brushes (PBs) and polymer nanocomposites (PNCs) are two common polymeric systems useful for antifouling applications. In a PB, polymers are grafted onto a surface at one end by physical or chemical means. At high grafting density, the polymer chains stretch away from the surface due to the molecular excluded-volume effects, producing a steric barrier resistant to non-specific adsorption of fouling species. Whereas hydrophilic polymers are often selected to maximize the steric repulsion, hydrophobic polymers such as fluoropolymers and poly(dimethylsiloxane) have also been proposed for antifouling control. In the latter case, the low surface adhesion energy renders polymer properties favorable for fouling release.[2] In comparison with PBs, the use of PNCs as antifouling materials is relatively new.[15–17] Addition of nanoparticles to a polymer matrix may result in enhanced mechanical properties and novel functions such as nanoparticle penetration into bacterial membranes or inactivation of enzymes. For instance, polymer composites containing Cu nanoparticles exhibit excellent antifungal properties.[18] Alternatively, protein-polymer composites may incorporate a broad range of the chemical and biological functionalities of proteins and polymers that can be utilized to minimize the binding affinity of fouling species thereby promoting fouling release.

The performance of polymeric materials for antifouling applications depends on a large number of parameters including the surface energy, chemical identity and stability of polymers, molecular architecture, polymer chain length, polydispersity and so forth. For example, the internal structure of a polymer brush is strongly affected by, in addition to the chemical composition and the solution condition, the polydispersity of polymer chains.[19] At a fixed grafting density and an average molecular weight of polymers, increasing the polymer polydispersity raises the average height of the brush but reduces the average chain stretching. Toward identification of key parameters for design and fabrication of antifouling materials has inspired myriad theoretical investigations. In order to understand the polymer surface behavior, one may use conventional theoretical methods ranging from phenomenological descriptions of colloidal forces to full atomistic molecular dynamics (MD) and Monte Carlo (MC) simulations. Statistical-mechanical studies of polymeric systems are mostly based on the scaling analysis,[20] polymer self-consistent-field theories (SCFT),[21] the integral-equation theories (IET),[22] and the classical density-functional theories (DFTs).[23] Among these theoretical methods, DFT is particularly proficient for investigating the properties of polymers potentially useful for antifouling applications. DFT takes root in a rigorous statistical-mechanical framework and most importantly, is directly applicable to both polymers and small molecules or ions in a typical aqueous environment.

Originally developed for electronic systems,[24] DFT becomes increasingly popular as an efficient computational tool for modeling polymeric systems. Fig. 1 shows the number of research articles published between 2002 and 2009 according to the Web of Knowledge® with "polymer theory" and various theoretical or simulation methods in the "topic" search. Publications with both "DFT" and "polymer" in the "topic" account for 7% of the total "polymer theory" papers published in 2002, and the percentage increases to 13% in 2009. In comparison to alternative computational methods, DFT combines the theoretical rigor with practical versatility, physical clarity, and numerical efficiency. Unlike molecular simulations, DFT directly deals with average properties of a thermodynamic system and thus avoids enumeration of the microscopic details and instantaneous fluctuations of individual particles. By expressing the intrinsic Helmholtz energy as a functional of the polymer density, DFT provides a self-consistent approach to predicting the structure and thermodynamic properties at uniform as well as inhomogeneous conditions. In comparison to conventional coarse-grained methods, DFT is able to account for microscopic details such as the molecular excluded-volume effects, associating interactions, van der Waals attraction, Coulomb forces, and inter- and intra- molecular correlations that are important for

Jianzhong Wu

Dr Jianzhong Wu is a professor of Chemical and Environmental Engineering and a cooperating faculty member of Applied Mathematics at the University of California, Riverside. He received his PhD in Chemical Engineering from the University of California, Berkeley, and MS and BE in Chemical Engineering and BS in Applied Mathematics from Tsinghua University, Beijing. Dr Wu's research is mainly concerned with development and application of statistical-mechanical methods, including density functional theory, for describing the physiochemical properties of soft materials.

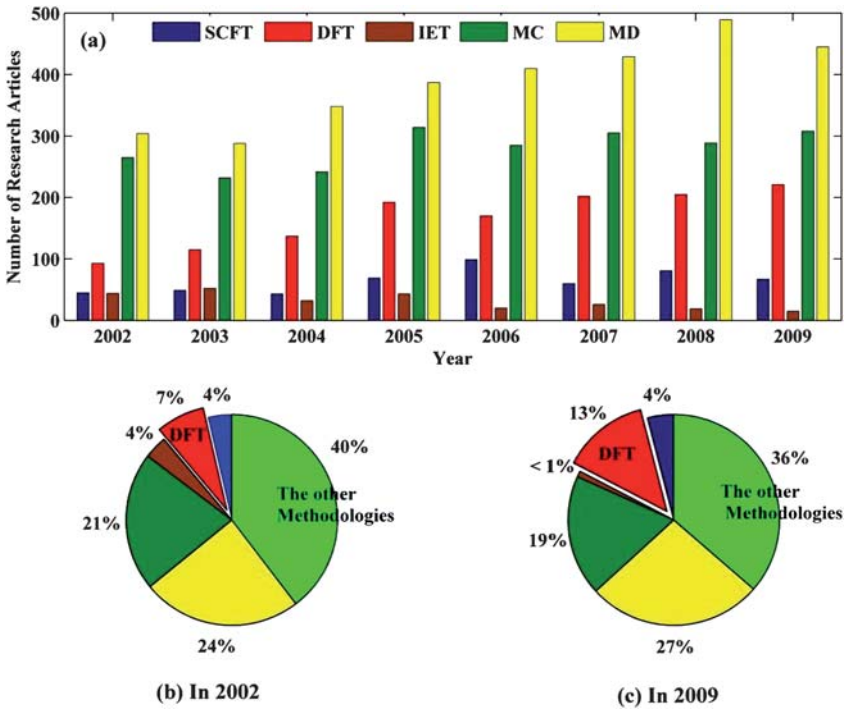

Fig. 1 (a) The number of articles published between 2002 and 2009 on theoretical polymer research by using SCFT (blue), DFT (red), IET (brown), MC simulation (dark green), and MD simulation (yellow). (b) Pie chart in 2002. (c) Pie chart in 2009. The data are from the ISI Web of Knowledge®.

understanding interactions of polymers with biological substances. The theoretical versatility and numerical efficiency of DFT makes it ideal for describing the interfacial properties of polymeric systems, in particular those involving multiple length-scales that are difficult to study by using alternative methods.

The purpose of this article is to review recent applications of DFT to polymeric systems that are potentially useful for surface fouling control. We begin with a brief overview of the basic concepts of DFT for polymeric systems. To minimize mathematical details, we discuss in the Appendix various strategies for formulation of the free-energy functionals of polymeric systems. Because of the nonspecific nature of biological systems, applications of DFT against biofouling are discussed within the context of "minimalist" models that only capture the basic features of polymeric systems and their surface behavior. Our emphasis is thus given to the capability of DFT for investigating various polymer-mediated interactions, nanoparticle self-organization in a polymer matrix, and the surface-induced behavior. The DFT predictions will be compared with results from conventional methods including molecular simulations. In particular, we will examine in detail how the surface behavior of polymeric systems is influenced by the polymer chain length, molecular architecture, chain-particle interactions, polymer-surface interactions and solvent effects.

2. Polymer density functional theory

Density functional theory (DFT) was originally proposed within the framework of quantum mechanics for describing the ground-state energy of electronic systems.[24,25] The central concept stems from a mathematical theorem, which states that for a system in the ground state or at equilibrium, the one-body external potential can be uniquely determined by the one-particle density distribution function. The mathematical framework is equally applicable to electronic and classical systems.[26–31] In the latter case, it asserts that the free energy is a unique functional of the one-body density distribution function and attains a minimum at equilibrium. For uniform systems, the one-body density distribution function becomes equivalent to the radial distribution function or the density distribution of particles near an imaginary "test particle".[32]

For classical systems, the basic concepts of DFT can be illustrated by considering a system containing N identical particles. Because the particles follow classical dynamics, the one-body density function (or density profile) is defined as

$$\rho(\mathbf{r}) = \left\langle \sum_{i=1}^{N} \delta(\mathbf{r} - \mathbf{r}_i) \right\rangle \quad (1)$$

where $\langle\rangle$ denotes the ensemble average, and δ is the Dirac function. For electronic systems, the one-body density profile can be related to the multi-body wave functions.[27] At equilibrium, the equilibrium density profile satisfies the variational principle:

$$\frac{\delta\Omega[\rho]}{\delta\rho(\mathbf{r})} = 0 \quad (2)$$

where Ω stands for the grand potential. From eqn(2) one can obtain the density distribution function and subsequently both the microscopic structure and thermodynamic properties of the system by following standard statistical-mechanical equations.[31] Because the grand potential and Helmholtz energy are related by the Legendre transform:

$$\Omega[\rho] = F[\rho] + \int d\mathbf{r}\rho(\mathbf{r})[V(\mathbf{r}) - \mu] \quad (3)$$

where μ represents the chemical potential, and $V(\boldsymbol{r})$ is an external potential, the essential task in application of DFT is to derive an analytical expression for the Helmholtz energy functional F.

For a polymeric system, the free-energy functional can be expressed in terms of the segment (or site) density as proposed first by Chandler, McCoy, and Singer (CMS),[33,34] or in terms of the polymer configurations as proposed first by Woodward.[35] In both cases, the free energy is formulated relative to that for a system of ideal chains with the same distribution of polymer configurations. While the two approaches are complementary to each other, they differ significantly in terms of the free-energy functional for ideal chains. According to the CMS-DFT, the ideal chains do not interact with each other but each polymer chain retains the full intramolecular interactions. As a result, the ideal Helmholtz energy includes a contribution identical to that corresponding to a monomeric system with the same density distribution, and a bonding free energy that accounts for the intramolecular correlations. For example, the ideal Helmholtz energy functional for a system of chain-like molecules is given by

$$\beta F^{\mathrm{id}} = \sum_{i=1}^{M} \int \mathrm{d}\mathbf{r}\rho_i(\mathbf{r})[\ln\rho_i(\mathbf{r}) - 1] + \beta F_{\mathrm{Bond}} \tag{4}$$

where each chain has M identical segments (or sites), $\rho_i(\boldsymbol{r})$ represents the density profile of segment i, and $\beta^{-1} = k_{\mathrm{B}}T$. In eqn(4), F_{Bond} includes contributions from both bonded and non-bonded interactions among segments in the same polymer chain. Because there is no exact analytical theory to represent the multi-body intramolecular interactions and the affiliated correlation effects, the ideal Helmholtz energy is generally unknown in CMS-DFT. At weakly inhomogeneous conditions, the bonding free energy is often approximated by a quadratic expansion relative to that corresponding to a uniform polymeric system of bulk density ρ_{b}:

$$\beta F_{\mathrm{Bond}} \approx -N(M-1)(\ln\rho_{\mathrm{b}} - 1) - \frac{1}{2}\sum_i \sum_j \iint d\mathbf{r}d\mathbf{r}' c_{ij}^{0}(|\mathbf{r}-\mathbf{r}'|)[\rho_i(\mathbf{r}) - \rho_{\mathrm{b}}][\rho_j(\mathbf{r}') - \rho_{\mathrm{b}}] \tag{5}$$

where N is the total number of molecules (chains) in the system, and $c_{ij}^{0}(r)$ represents the site-site direct correlation function of the ideal uniform system (that entails all intramolecular interactions).

Within the framework of the polymer DFT proposed by Woodward,[36] the ideal polymer chains are defined such that both the intermolecular and non-bonded intra-molecular interactions are neglected. In that case, the ideal free energy can be formally expressed as a functional of the configurational density $\rho_{\mathrm{M}}(\boldsymbol{R})$and the bonding potential $V_{\mathrm{B}}(\boldsymbol{R})$:

$$\beta F^{\mathrm{id}}[\rho_{\mathrm{M}}(\boldsymbol{R})] = \int \mathrm{d}\boldsymbol{R}\rho_{\mathrm{M}}(\boldsymbol{R})[\ln\rho_{\mathrm{M}}(\boldsymbol{R}) - 1] + \beta\int \mathrm{d}\boldsymbol{R}\rho_{\mathrm{M}}(\boldsymbol{R})V_{\mathrm{B}}(\boldsymbol{R}) \tag{6}$$

where $\boldsymbol{R} \equiv (\boldsymbol{r}_1,\ldots,\boldsymbol{r}_M)$ stands for the configuration of a polymer chain with M segments. In this case, numerical implementation of the polymer DFT involves multi-dimensional integrations that must be evaluated either by using the Green functions ("propagators" as in a typical polymer self-consistent-field theory[21]) or by using single-chain molecular simulation.[37,38] For example, Yethraj and Woodward[39] presented a hybrid DFT by treating the ideal free-energy functional exactly *via* a single-chain Monte Carlo (MC) simulation and the non-ideal free energy through a weighted-density approximation.[40–42] While single-chain simulation avoids direct evaluation of the multi-dimensional integrations and enables direct applications of the DFT to polymers with nonlinear molecular architecture, the hybrid method is computationally expensive. The heavy computational cost is closely related to the single-chain simulation that is coupled within a numerical iteration to solve the variation equation (*viz.* eqn (2)). For polymer models with only the nearest-neighbor bonding potential, the computational efficiency can be drastically improved by using a hierarchical algorithm.[38]

Alternative DFT approaches have also been proposed to derive the free energy of polymeric systems. For example, Chapman and coworkers[43–45] expressed the polymer Helmholtz energy in terms of that corresponding to a mixture of atomic fluids plus an association energy arising from bond formation. The monomer-based approach can be understood as an extension of the statistical associating fluid theory (SAFT) for bulk systems.[46,47] Recently, Woodward and Forsman[37] suggested that the polymer free-energy functional can be expressed in terms of the distribution of polymer end segments rather than the density profiles of all segments as in CMS-DFT or the multi-dimensional configurational density as in the polymer DFT originally proposed by Woodward.

The excess free energy functional accounts for the non-bonded interactions and the affiliated density correlation effects. In other words, the excess free energy functional represents thermodynamic properties beyond that corresponding to an ideal system. In general, the excess Helmholtz energy functional can be formulated by perturbation expansions relative to a reference system that has the same segmental density profiles (but different interaction potentials) or the same interaction potentials (but with different polymer density profiles).[23] Mathematically, the former approach is equivalent to the closures of the integral-equation theory of uniform fluids; and the latter amounts to the perturbation theories.[48]

For polymers in an aqueous environment, the non-bonded interactions between polymer segments include multiple contributions arising from the polymer excluded-volume effects, hydrophobic and hydrophilic associations, van der Waals interactions, and Coulombic interactions.[49] Whereas a quantitative representation of these intermolecular forces remains a grand challenge, semi-empirical models are often available to represent various components of water-mediated interactions. With a semi-empirical representation of the intermolecular forces, analytical expressions for the excess free energy functional can be derived that compare favorably with molecular simulations.[23] In the Appendix, we outline some useful strategies for formulation of the excess free energy to represent contributions due to various components of the intermolecular forces. For systems with sufficient chemical details, the semi-empirical approaches are often capable of quantifying polymeric interactions with biological substances.[50,51] In applications of the DFT for antifouling systems, however, quantitative predictions are more difficult due to unknown local compositions of biological species and due to the unavailability of reliable experimental data for calibration of the model parameters. As a result, the DFT predictions discussed in this work are mostly based on

"minimalist" models of polymer (*e.g.*, hard-sphere chains) and biological species (*e.g.*, spherical particles). Theoretical investigations based on chemically non-specific model systems may nevertheless provide valuable insights for development of universal antifouling strategies.

3. Antifouling brushes

3.1 Brush structure

The early literature on antifouling control is primarily concerned with hydrophilic brushes and their interactions with proteins or colloidal particles in an aqueous environment. In order to describe the polymer steric repulsion, the conformation of grafted polymers and the polymer concentration profile are often represented by simple theoretical models that take into account the chain elasticity and the segmental excluded-volume effects. To recapture the essential features, Fig. 2 shows the distribution of polymer segments predicted by the DFT in comparison with those from the scaling analysis[52] and from an analytical theory by Milner, Witten and Cates (MWC).[53] For simplicity, here we consider a model brush of tangentially-connected hard-sphere chains with one end grafted on a planar surface that is "neutral" to the polymer segments, *i.e.*, there is no interaction energy other than the excluded-volume effect. For the results shown in Fig. 2, each polymer chain consists of M=200 spherical segments of diameter σ and the surface tethering density is $\rho_g\sigma^2 = 0.4$, corresponding to that for a highly stretched polymer brush.

According to the MWC theory, the density profile of polymer segments is a parabolic function of the distance from the tethered surface (z)

$$\rho(z) = \frac{\pi^2}{8N^2}\frac{(L^2 - z^2)}{v\sigma^2} \tag{7}$$

where N is the number of polymer (Kuhn) segments of diameter σ, $v = 2\pi\sigma^3/3$ is the segmental virial coefficient. The brush thickness is determined from

$$L/\sigma = N\left(\frac{8\rho_g\sigma^2}{\pi}\right)^{1/3} \tag{8}$$

where ρ_g denotes the polymer tethering density. The MWC theory predicts the polymer density profile in quantitative agreement with that from the full polymer self-consist-field theory (SCFT).[54] The scaling theory by de Gennes hinges on the flat density assumption ("Box model"), *i.e.*, the density of polymer segments is uniform within the brush. By balancing the elastic energy and the excluded-volume effects, it yields a simple expression for the brush thickness

$$L/\sigma = N(\pi\rho_g\sigma^2/3)^{1/3}. \tag{9}$$

Fig. 2a shows that the scaling theory gives a brush thickness in near perfect agreement with the DFT calculation. By contrast, the parabolic density profile predicted by the MWC theory shows noticeable discrepancy from the DFT in both proximal (Fig. 2b) and distal (Fig. 2a) regimes of the polymer brush.

The MWC theory and the scaling analysis do not give an oscillatory density profile in the proximal region because both methods neglect the packing effects of polymer segments. The

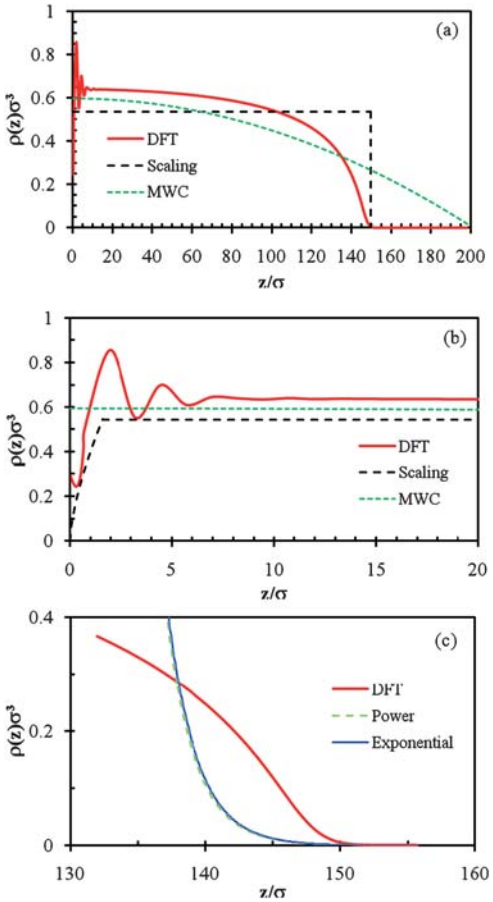

Fig. 2 The distribution of polymer segments in a polymer brush predicted by the DFT, by the strong-stretching theory of Milner, Witten and Cates (MWC), and by the scaling analysis of Alexander and de Gennes (Scaling). Here the tethered polymers are represented by tangentially-connected hard-sphere chains; each chain contains 200 spheres of diameter σ and the surface grafting density is $\rho_g\sigma^2 = 0.4$. (a) The overall density profiles of polymer segments; (b) Segment density closest to the surface ("proximal regime"); (c) Segment density furthest from the surface ("distal regime"). "Power" and "Exponential" refer to fitting of the DFT results with the power law or exponential functions.

discrepancies in the distal regime are mainly due to the "ansatz" of constant density or of parabolic density used in these simple models. While the numerical success of the scaling analysis is most likely due to cancellation of errors, Fig. 2 offers a partial explanation why the simple scaling laws sometimes outperform the SCFT.[55] Near the grafting surface, the polymer DFT predicts strong oscillation of polymer density due to the segmental excluded-volume effect (Fig. 2a). As suggested by neutron scattering experiments,[56] the polymer density decays neither exponentially nor in a power law to the bulk concentration at the brush edge (Fig. 2c). While direct detection of the microscopic structure near a polymer surface is extremely difficult in experiments,[57] the DFT predictions appear in good agreement with molecular simulations.[58]

Fig. 3 shows some further details of the polymer structure for the same model brush and the dependence of the brush thickness on the tethering density. Noticeably, the end-segment density

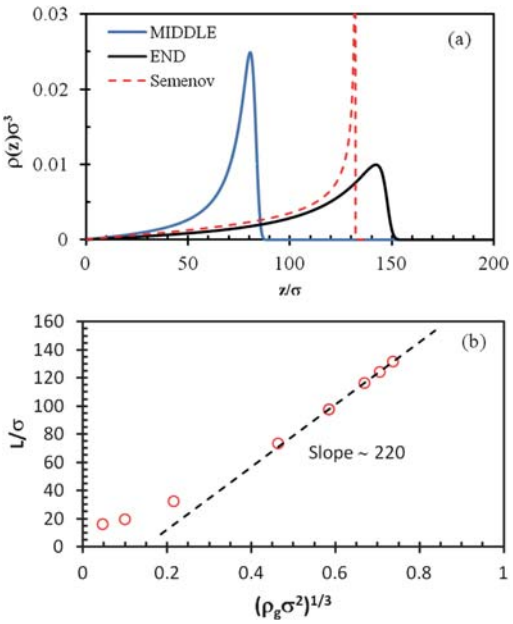

Fig. 3 (a) The density profiles for the middle and end segments of the polymer brush considered in Fig. 2. The dashed line shows the prediction of Semenov's theory.[161] (b) Brush thickness *versus* the polymer grafting density. The line shows the scaling relation by de Gennes.[61]

shows no divergence near the brush edge.[58] At the strong stretching limit, the brush thickness varies with the grafting density closely following the scaling relation, $L/\sigma = M(\pi\rho_g\sigma^2/3)^{1/3}$. In the light of the theoretical simplicity of the scaling analysis, its quantitative agreement with the DFT predictions is truly remarkable.[59,60]

3.2 The steric repulsion

The steric repulsion from a polymer brush has been calculated by scaling analysis,[61] SCFT,[62–64] and molecular simulations.[58] With a few fitting parameters, both the scaling equations and the SCFT are able to quantitatively reproduce the interaction force between a brush and a flat surface obtained from experiments or from simulations.[65,66] Qualitatively, similar steric force profiles can be reproduced from the DFT calculations. To illustrate, we show in Fig. 4 the potential of mean force (PMF) between a brush of hard-sphere chains and spherical particles of different sizes. The system mimics interactions between a polymer brush and particles in a good solvent. Here the polymer chain length is $M = 100$ and the reduced grafting density is $\rho_g\sigma^2 = 0.4$. The steric potential predicted by the DFT is very close to those from the SCFT.[63,67] Because the particle and polymer segments are in different length scales, strong oscillation of the segment density near the surface is not manifested in the force profile. Fig. 4(b) shows the repulsive energy when a particle is in contact with the bare surface. The excellent fitting suggest that the particle inclusion energy can be accurately represented by the solvation equation from the morphometric thermodynamics.[68] Instead of a linear dependence on the particle radius,[60] the DFT predictions indicate that the particle inclusion energy depends on the particle volume, surface area and curvature.

The brush structure and its interaction with colloidal particles can be drastically altered by attractive interactions among the polymer segments and the surface. Schematically, the particle-brush interaction can be classified into three generic modes depending on the particle size and the interaction energy: primary, secondary, and ternary adsorptions.[69,70] In primary adsorption, particles diffuse through the polymer brush and are adsorbed onto the surface. Secondary adsorption occurs, when particles are primarily adsorbed at the brush-solvent interface and affect the properties of the surface significantly. In ternary adsorption, particles diffuse into the brush and are trapped by the polymer chains. Evidently, the particle size is an important factor in determining the adsorption mechanism. At the same surface energy, big particles tend to adsorb at the outer rim of the brush, whereas small particles are most likely to penetrate into the polymer film, resulting in higher primary adsorption.[71] The strength of primary adsorption is dominated by the short-ranged attraction between particles and the substrate and the adsorption can be suppressed by increasing the polymer grafting density. The secondary adsorption is mainly due to intermolecular attractions between the polymer chains and particles. In that case, adsorption of particles on the substrate can be minimized by reducing the grafting density but increasing the brush thickness.

In addition to the particle size and surface energy, the interaction between the tethered polymers and the substrate has a significant effect on non-specific particle adsorptions. For polymers attracted to the surface, the steric barrier disappears

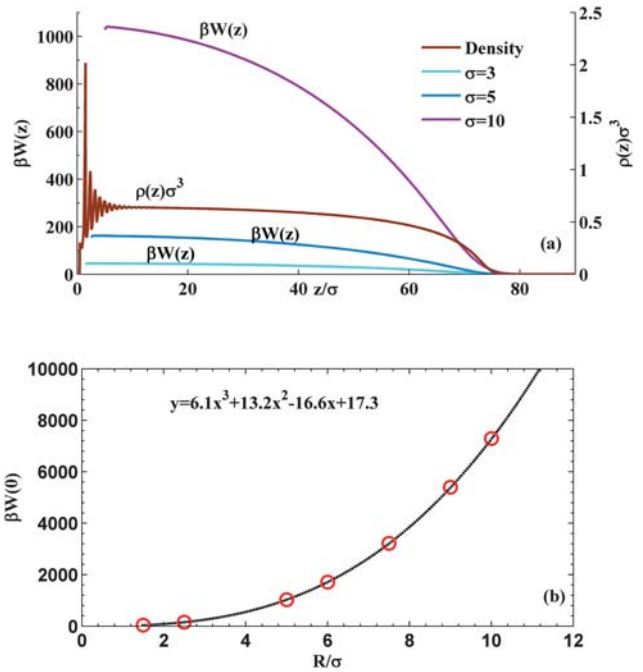

Fig. 4 (a) The potential of mean force between a polymer brush and particles of different diameters. The right axis shows the density profile of the polymer segments. Except the chain length ($M = 100$), the polymer parameters are identical to those shown in Fig. 2. (b) The brush contact energy of spherical particles predicted by DFT. The dashed line shows a correlation of the surface potential with the morphometric thermodynamics.

and particle adsorption is in direct competition with the polymer. Increasing the surface affinity of tethered polymers minimizes direct non-specific adsorption and favors foul release. On the contrary, polymers repelled from the surface generate strong steric repulsion but less surface coverage. In that case, particles penetrating the polymer film result in primary adsorption. Because of the lack of a reliable theory to describe non-specific interactions among polymers and surfaces in an aqueous solution, few DFT investigations have been reported on quantitative predictions of particle-brush interactions against biofouling.

3.3 Architecture of the tethered chains

The efficiency of polymer brushes for antifouling applications depends on a broad range of parameters including the polymer chain length, chain architecture, polymer-particle interaction energy, polymer-surface interactions, and solution conditions. Polymer architecture may prove to be the most significant parameter in design of new strategies to eliminate biofouling. For example, brushes made of amphiphilic block copolymers or polymer mixtures provide a unique mechanism for resistance of fouling substances.[72–74] The high antifouling efficiency of these materials is in part due to the fact that surface coated with an amphiphilic block copolymer becomes hydrophobic when they are in contact with Ulva spores and tunes into hydrophilic when they are close to Navicula.[73] Ulva and Naviculas are two predominant fouling microorganisms responsible for formation of marine biofilms, one of which adheres strongly to hydrophobic surfaces and the other to hydrophilic surfaces.[73] Polymer with more complicated architectures, such as capsular polysaccharides, is likely even more efficient for inhibition of non-specific adsorptions.[75]

The qualitative behavior of microorganism adhesion onto an amphiphilic polymer surface can be captured by a "minimalist" model that depicts the grafted amphiphilic side chains as freely-joined chains of hard spheres and microorganisms as spherical testing particles. Fig. 5(a) shows the density profiles of amphiphilic polymers at three different substrates. Near a neutral or a hydrophilic surface, the brush out surface is hydrophobic but near a hydrophobic surface it turns into hydrophilic. The numerical results affirm that tethered amphiphilic chains are able to reconstruct the polymer conformation in response to different surfaces. Fig. 5(b) shows the polymer-mediated potentials for hydrophobic and hydrophilic testing particles whose diameter is five times that for polymer segments ($\sigma_C = 5\sigma_P$). Whereas a hydrophobic particle shows a damped attraction to hydrophobic surface or polymer block, the block copolymer introduces a strong repulsion close to the substrate to all surfaces, facilitating steric repulsion and easy removal of biofouls.

Xu and Cao[76] examined in detail the effect of the polymer chain architecture on the adsorption of colloidal particles. They considered surfaces grafted with polymers of a wide variety of molecular architectures, including linear, star, branched, and dendritic structures. By studying the adhesion behavior of colloidal particles interacting with these polymeric surfaces, they

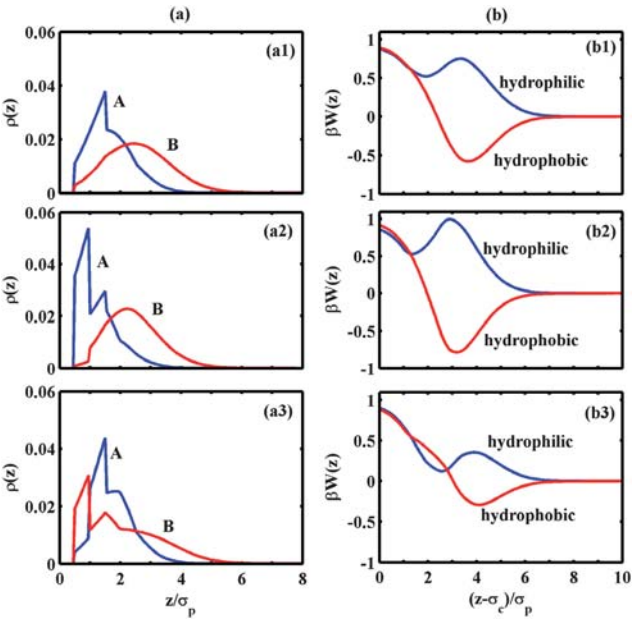

Fig. 5 **(a)**: Density profiles of block-like amphiphilic molecules (A is hydrophilic and B is hydrophobic) at (a1) an inert surface, $\varepsilon_{AW}=\varepsilon_{BW}=0$; (a2) a hydrophilic surface, $\varepsilon_{AW}=1$, $\varepsilon_{BW}=-1$; and (a3) a hydrophobic surface, $\varepsilon_{AW}=-1$, $\varepsilon_{BW}=1$. Here ε stands for the reduced interaction energy between any pairs of segments/wall represented by the square-well potential. **(b)**: Polymer-mediated potential for a hydrophilic (blue) and a hydrophobic (red) testing particle near different surfaces where the substrate is (b1) inert; (b2) hydrophilic; and (b3) hydrophobic. In all cases, each amphiphilic chain has 10 segments of equal size; the first 5 segments close to the surface (block A) are hydrophilic, and the next 5 segments (block B) are hydrophobic. $\varepsilon_{CA}=1$and $\varepsilon_{CB}=-1$ for the hydrophilic particle, and $\varepsilon_{CA}=-1$ and $\varepsilon_{CB}=1$ for the hydrophobic particle. The grafting densities are fixed at $\rho_g\sigma_p^2=0.01$, and the diameter of polymer segments is used as the unit length, *i.e.*, $\sigma_{ij}=\sigma_p=1$. The energy parameters are set as $\varepsilon_{AA}=\varepsilon_{BB}=1$, $\varepsilon_{AB}=-1$, *i.e.*, the hydrophobic/hydrophilic segments attract each other but there is a repulsion between segments of different hydrophobicity.

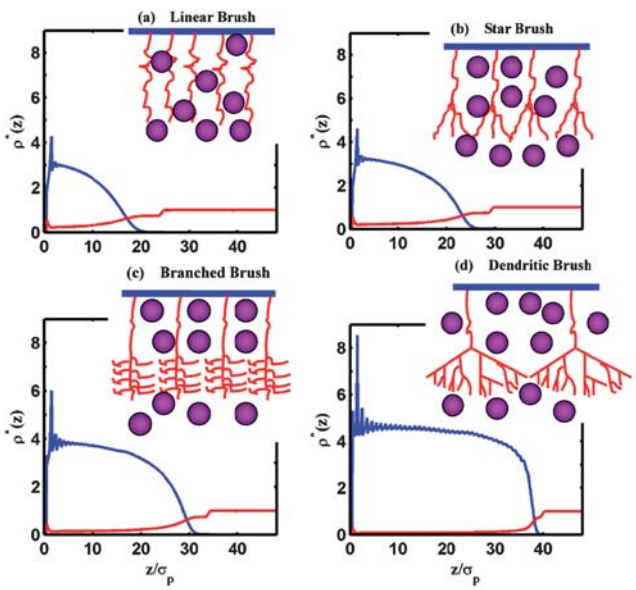

Fig. 6 Effect of polymer architecture on the density profiles of PBs (blue line) and colloids (red line). (a) Linear, (b) Star, (c) Branched, (d) Dendritic architecture. Reprinted with permission from ref. 76.

found that polymer chains with complex molecular architecture are in general much more effective than linear polymers in preventing colloidal adsorption. For example, Fig. 6 shows the density profiles of tethered polymers of various molecular architectures in contact with adsorbing particles. While the linear polymers are relatively inefficient to prevent the primary adsorption of colloidal particles, adsorption within the brush is reduced as more branches are introduced into the tethered chains. Because the side chains could effectively prevent penetration of particles in the brush, polymers with complex architecture are favored for minimizing both the primary and the ternary adsorptions.

3.4 Surface phase transitions

DFT has also been applied to studying condensation and layering transitions of adsorbed species near brush surfaces.[77,78] For example, Zhou *et al.*[79] examined the structure and phase behavior of a particle-block copolymer mixture confined between two polymer-grafted surfaces. With increasing the particle concentration, they observed that the composite film undergoes a series of phase transitions reflecting a competition between formations of various mesoscopic phases and wetting transitions. Jain *et al.*[80] investigated the interactions between two polymer-grafted monolayers in the absence/presence of free polymer. In the absence of free polymers, the interaction force is always repulsive due to the steric hindrance of the monolayers. The situation is more complicated when the two grafted monolayers are filled with free polymers. In that case, the surface force exhibits an attractive minimum depending upon the polymer grafting density, the relative chain lengths, and the excluded-volume of polymeric molecules. The attractive minimum is observed only when the size ratio of free and tethered polymers, $\alpha = N_f/N_g$, is beyond a critical value, where N_f and N_g stand for the degrees of polymerization of the free polymers and grafted polymers, respectively.[80]

The phase behavior of a polymer brush is directly related to the solvent quality. A poor solvent condition leads to self-association of the grafted polymers and brush compression. In a good solvent, favorable interaction between the polymer segments and solvent molecules results in the brush extension. Whereas the potential of mean force (PMF) between a particle and the polymer brush is purely repulsive in a good solvent, it shows a midrange attraction in a poor solvent. According to recent DFT calculations,[81] addition of only 20% of well-solvated chains to a poorly solvated brush is sufficient to change the PMF from attraction to repulsion.

3.5 The curvature effect

Polymer brushes on a curved interface mimics many important systems such as star polymers, polymers grafted on colloidal particles or curved membranes.[82–86] An accurate description of the effect of interfacial curvature is crucial to understand the polymer microscopic structure and the brush-mediated colloidal interactions. A major influence of the surface curvature arises from the gradual increase of the volume accessible to the tethered chains as the distance from the surface increases. Because the polymers stretch less far from the surface, the brush is less swollen in comparison to that of a planar brush at the same grafting density.[87]

Whereas relatively few DFT calculations have been published on the interaction between a particle and a curved brush,[64] some insightful conclusion can be drawn by considering the brush-brush interactions. For example, Frischknecht[88] studied the PMF between two nanorods grafted with homopolymer chains immersed in a polymer melt that is identical to the tethered chains. The polymer-mediated potential was found non-monotonic; it is attractive at intermediate separations but exhibits a steep repulsion when the two brushes come into contact with each other. A similar behavior was predicted for carbon nanotubes (CNT) dispersed in a solution of ionic surfactants.[89] Fig. 7 shows the DFT predictions for the equilibrium density profiles of the head segments (Fig. 7a), counterions (Fig. 7b, left), and the tail segments (Fig. 7b, right) around two parallel CNTs with center-to-center distance equal to 2.05 nm. According to the

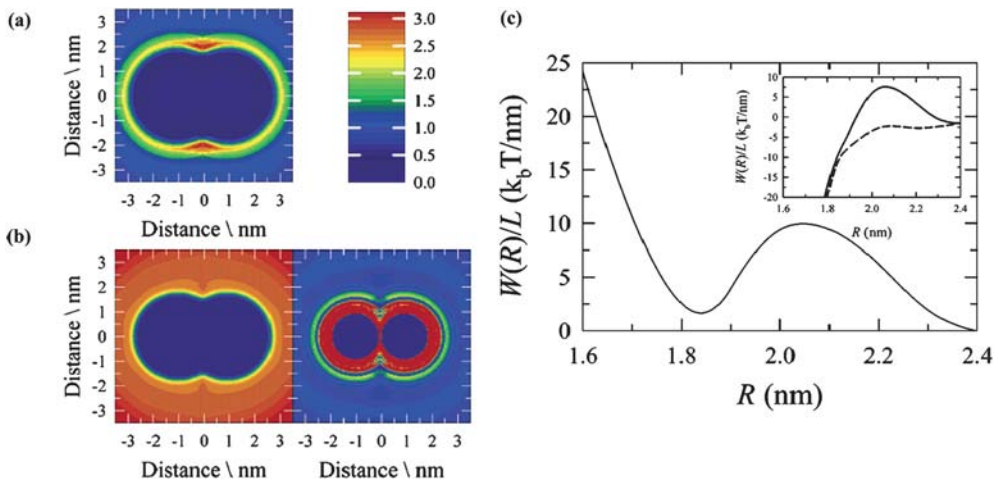

Fig. 7 Surfactant mediated potential for nanotubes. Density profiles of (a): head segments, (b) left: counterions, and (b) right: tails segments. (c) Surfactant mediated potential of mean force (PMF). Inset: Total and tube-tube PMFs are plotted with solid and dashed lines, respectively. Reprinted with permission from ref. 89.

density profiles, the hydrophilic heads are primarily located away from the CNT surfaces, while hydrophobic tail segments are strongly aggregated near these surfaces. Furthermore, the width of the density profiles of the tail segments is about 1 nm, indicating that the surfactant tails are randomly arranged on the CNT surfaces rather than strongly extended into the bulk. Fig. 7(c) shows the PMF mediated by ionic surfactants over a range of CNT separations. The profiles exhibit a pronounced minimum around 1.85 nm, followed by increasingly steep repulsion at smaller separation. As the two CNTs are dragged together from a large separation, the two respective layers of like-charged heads start repelling each other, resulting in an energy barrier around 2 nm. As the separation between two CNTs is further reduced, the head segments of the surfactant molecules cannot fit between the two tubes. In this case, the tail segments find themselves in an energetically favorable position because they experience a strong attraction to both tubes. The bridging surfactants lead to a strong attraction, which manifests itself as a minimum around 1.85 nm. At even shorter separations, the bridging attraction disappears and the PMT is dominated by the steric repulsion.

3.6 Patterned brushes

A nanopatterned brush (NPB) is formed by grafting polymers onto a nanostructured substrate. The symmetry and the length scale of the substrate pattern render novel brush properties potentially useful for fouling resistance.[90–92] As for polymers grafting to a homogeneous surface (*i.e.*, regular brushes), one may use the DFT to describe the monomeric densities of a NPB in the directions parallel and perpendicular to the grafted surface. For example, Fig. 8 shows the density profiles of two parallel NPBs by increasing the separation (L) between neighboring patterned arrays from 0 to 25 σ_p, where σ_p is the diameter of a polymer segment. At $L = 0$, the density contour is uniform in x direction and exhibits a highly oscillatory profile in z direction. With increasing brush distance L, the contour maps show that the behavior of NPBs is mainly determined by a competing influence of the aspect ratio (L/P, P is the pattern size) and the polymer architecture. To a certain degree, the surface morphology is similar to adsorption of polymers on nano-patterned surfaces.[93–96] Further theoretical investigations, especially on the effect of the surface pattern on colloidal forces, may provide useful insights for preparation of NPBs against fouling.

3.7 Tethered polyelectrolytes

Polyelectrolytes bear electrostatic charges on the polymer backbone. The presence of long-ranged electrostatic interactions makes a polyelectrolyte brush (PEB) potentially more effective for antifouling applications than an uncharged brush.[97] However, different from a neutral brush, the structure and interfacial behavior of a PEB are highly sensitive to the ionic valence of counterions and salt concentration.[98] As a result, a good understanding of the surface behavior of PEBs is critically important for their applications.

Depending on the ionic strength, PEBs are often categorized into osmotic brushes and salted brushes.[98] An osmotic brush corresponds to a PEB at a low salt concentration. In this case, the polymer chains are highly stretched due to the electrostatic repulsion and the brush swelling reflects a balance of the polymer elastic energy and the osmotic pressure of counterions. According to the scaling analysis,[98] the brush thickness depends linearly on the chain length, relatively insensitive to the grafting density and salt concentration. At high salt concentration, a PEB is called a "salted brush". In that case, the brush swelling is also determined by a balance of the polymer elastic energy and ionic osmotic pressure. But unlike the osmotic brush, the ionic concentration within a salted brush is mainly determined by the added salt concentration. Approximately, the thickness scales with the salt concentration in a power of $-1/3$ and with the grafting density in a power of 1/3.[99]

The swelling and microscopic structure of a PEB is extremely sensitive to the valence of counterions. For example, when a PEB is immersed in a solution containing trivalent counterions, electrostatic interaction may lead to a self-organization of the

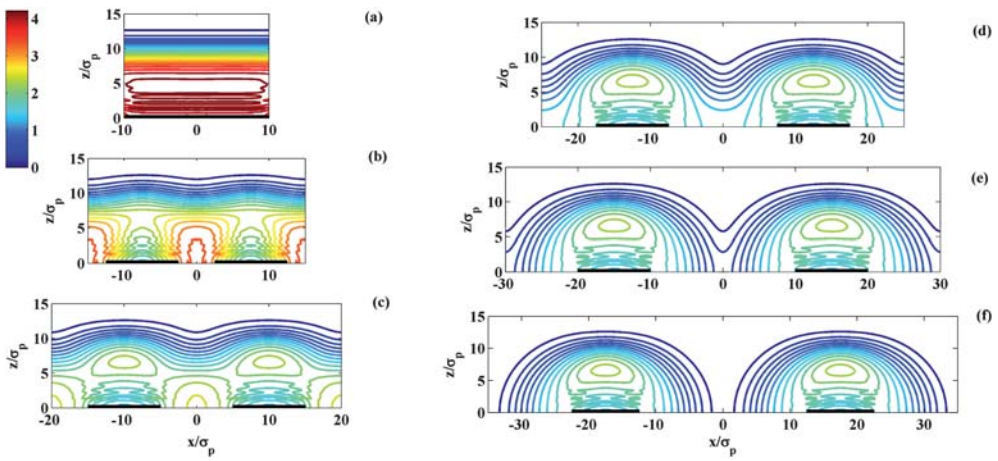

Fig. 8 Density contour maps of nanopatterned brushes in x-z plane. The contours are normalized by the grafting density, and are drawn in a level of 0.2. The separations between neighboring pattern array are (a) $L = 0$, (b) $L = 5\ \sigma_p$, (c) $L = 10\ \sigma_p$, (d) $L = 15\ \sigma_p$, (e) $L = 20\ \sigma_p$and (f) $L = 25\ \sigma_p$. The pattern size is fixed at $P = 10\sigma_P$. The polymer chain length is $N = 20$ and the grafting density in the patterns is $\rho_p\sigma_p^2 = 0.1$. The boundary in x direction is periodic.

counterions into a crystalline-like structure.[100] Because of the correlation effect, the local electrostatic potential exhibits a layer-by-layer charge inversion. The drastic difference in the swelling behavior of a PEB in a multivalent solution and that in a monovalent solution can be attributed to a competition of the counterion-mediated electrostatic attraction between polyions with the excluded-volume effect of all ionic species.[101]

The presence of multivalent counterions often results in a PEB collapsing at an intermediate grafting density and reswelling at higher grafting densities. At an intermediate grafting density, the brush collapses when the counterion-mediated attraction overcomes the excluded-volume effect. At high grafting densities, the brush re-swells because of the reduction of counterion-mediated attraction arising from correlation effects. To account the curvature effect, Ni *et al.*[102] investigated the swelling behavior of a spherical PEB in a solution containing oppositely-charged linear polyelectrolytes. The results show that with increasing the concentration of free polyelectrolytes, the spherical PEB undergoes a transition from swelling to collapse and to reswelling, very much the same as that in the presence of multivalent counterions.

Interaction of a PEB with colloidal particles depends strongly on the swelling and the electric properties of the brushes. At high salt concentration, the polyions are near perfectly neutralized by counterions and the electrostatic interaction manifests itself only in the chain stretching. In this case, the distribution of polymer segments and the brush-mediated steric repulsion are very similar to those corresponding to a neutral brush.[103,104] At low salt concentration, the long-range interaction between a charge particle and a PEB is dominated by direct electrostatic forces. Because the surface electrostatic potential extends significantly beyond the brush layer, the long-range electrostatic and short-range steric interactions can be described, respectively, by the classical theories for electric double layers and for neutral polymer brushes.[98]

4. Polymer nanocomposites

Loaded with heavy metals,[105] antibiotics,[106] small molecule biocides[107] or halogen species,[6] polymer nanocomposites may show outstanding antibacterial properties. This unconventional approach is in particular attractive if the imbedded particles can penetrate through bacteria membranes and inactivate enzymes. A number of reports have indicated the potential applications of polymer nanocomposites against biofouling and cell adhesion.[2] For rational design of such materials, DFT calculations will provide insights on nanoparticles dispersion in a polymer matrix, thermodynamic stability, as well as the release rate of nanoparticles into a changing environment. The theoretical results will also be beneficiary in developing novel strategies for preparing non-fouling surfaces.

4.1 Polymer-mediated interactions

As well documented, nanoparticles dispersed in a polymer solution experience an attractive interaction due to depletion of polymers between the particles. The depletion potential is influenced by the polymer molecular weight and particle size, polymer concentration, chain architecture including length and stiffness, and polymer polydispersity, surface energy as well as the polymer interaction solvents.[108] While the polymer-mediated potential between two planar surfaces or two small particles is relatively straightforward to calculate, the interaction at the intermediate length scales is not described by conventional colloidal theories. By using the DFT and the potential distribution theory, Li and Wu calculated the interaction between colloidal particles of arbitrary size.[109] They found that the Derjaguin approximation works reasonably well at high polymer concentration even for small colloidal particles, but it becomes qualitatively incorrect at low polymer concentration. The Derjaguin approximation deteriorates as the polymer concentration decreases because it neglects the curvature effect, which is most significant when the interaction range becomes comparable to the particle size. Similar DFT methods were used to examine in detail the effects of polymer packing fraction, degree of polymerization, polymer/polymer size ratio, colloid/polymer size ratio on the depletion interactions.[55,110]

One major advantage in application of the DFT for calculating polymer-mediated colloidal forces is that the equations developed for linear polymers can be directly applicable to systems containing polymers with complicated molecular architectures. For example, both experiments and theoretical calculations indicate that the interaction between two highly stretched telechelic brushes is primarily repulsive. However, a weak attraction was observed when two telechelic brushes are at the classical contact, *i.e.*, the separation between two brushes is about twice the brush thickness.[111,112] Cao and Wu[113] employed a DFT method to examine the origin of this weak attraction with explicit consideration of the surface-adhesive energy and the segment-level interactions. The DFT is able to capture the depletion-induced attraction in the presence of weakly adhesive polymers and the steric repulsion between compressed brushes. Moreover, the weak attraction at the classical contact is clearly presented in the cases of strongly adsorbed telechelic polymers. By comparing the solvation forces between telechelic brushes with those between the brushes formed by surfactant-like polymers and with those between two asymmetric surfaces mediated by telechelic polymers, it was found that the weak attraction between telechelic brushes is primarily caused by the bridging effect. Similarly, Woodward *et al.*[114] studied the surface forces introduced by star-shaped polymers confined in a slit pore. As the surfaces are moved together, the polymer depletion effect gives rise to a repulsive barrier with the magnitude scaled linearly with the number of polymer arms. A more complex polymer architecture would magnify the depletion effect.[76] The intrinsic rigidity of polymers also has a significant effect on the surface force. Increasing the intramolecular chain stiffness from fully flexible to moderately stiff chains leads to an increased free energy barrier of the depletion interaction.[115]

The distribution of polymers near a surface and polymer-mediated interactions are directly related to the solvent conditions.[116] The solvent effect is particularly important if the polymer segments and solvent molecules experience a long ranged potential from the surface.[116] In addition to the surface energy, the polymer-mediated forces may depend on the polymer polydispersity.[117] Whereas for flexible polymers the effect of polydispersity on the depletion attractions is relatively small, the effect is quite significant for stiff polymers particularly at high

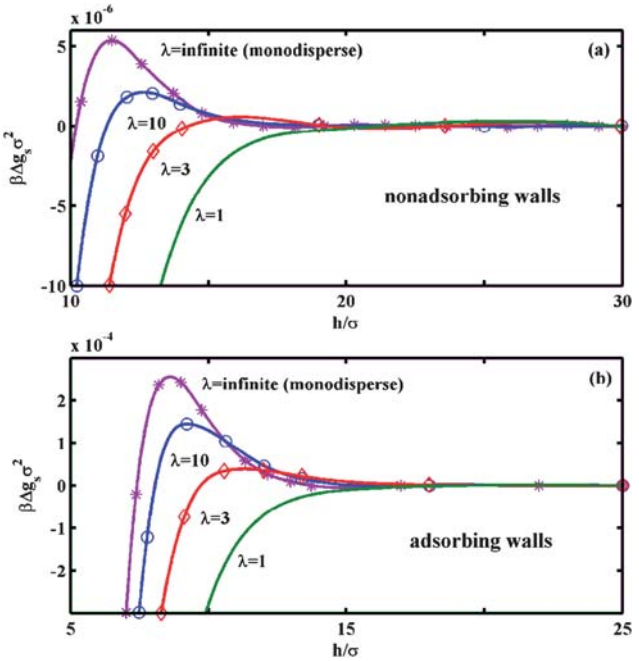

Fig. 9 Polydispersity-induced attractive interactions between (a) non-adsorbing walls, and (b) adsorbing walls. Reprinted with permission from ref. 131.

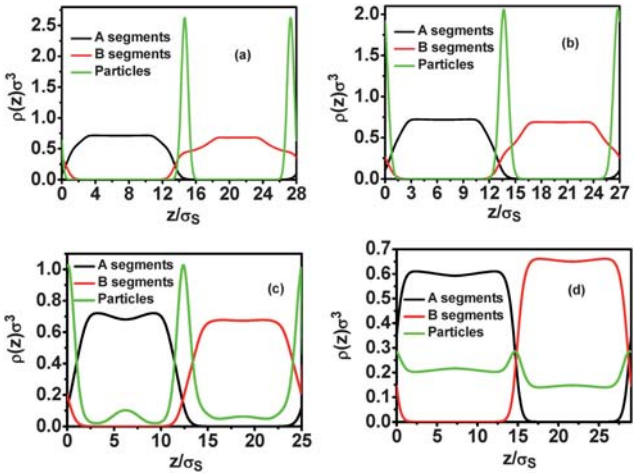

Fig. 10 The density profiles of the polymeric segments ("A" and "B") and nanoparticles for $\varepsilon^*_{AA}=\varepsilon^*_{AP}=0.05$. Particle size is $\sigma^*_P=7$ in (a), $\sigma^*_P=5$ in (b), $\sigma^*_P=3$ in (c) and $\sigma^*_P=1$ in (d). Packing fraction for the polymer is 0.32, and that for the particles is 0.05. The polymer chain length is $N=100$. Reprinted with permission from ref. 119.

polymer concentrations.[118] The chain stiffness magnifies the polydisperse effect due to the depletion of long-chain molecules from the surfaces, leading to a longer-range osmotic attraction. In addition to the chain stiffness, polydispersity has a strong impact on polymer depletion near adsorbing surfaces. The adsorption of long polymers at both surfaces results in an increase of the bridging attraction.

Fig. 9 shows the effect of polydispersity on polymer-induced attraction between two walls. The polydispersity index (λ) describes the width of the distribution of molecular weight: $\lambda=1$ corresponds to uniformly polydispersed polymers, and as λ increases, the polymers become more monodispersed. For interaction between non-adsorbing surfaces, the polymer-mediated potential is initially repulsive because the configurational entropy of polymer chains is reduced as the separation between the surfaces is decreased. As the polydispersity increases (*i.e.*, λ decreases), the steric barrier diminishes and the depletion attraction becomes longer-ranged. In the case of adsorbing surfaces, the trend is similar but the attractive interaction at small separation is drastically increased due to the bridging effect. Because the bridging is directly related to the polymer chain length, the polydisperse effect is most significant at large separations.

4.2 Nanoparticle distribution

Block copolymers are commonly used as a template to control the PNC structure. The particle distribution within the block copolymer matrix is primarily determined by the particle size and surface energy. For example, within the lamellar structures of symmetric block copolymers, neutral particles tend to localize at the microdomain interface and reduce the lamellar thickness.[119] Particles that are energetically biased to a particular microdomain expand the block copolymer lamellar structure. Because the DFT can be directly used to describe particles and block copolymers within a single molecular model, it is convenient to predict the morphology of a PNC and how that varies with the particle size and surface energy. Fig. 10 shows, for example, the density distributions of block copolymer segments (A and B) and nanoparticles in a model composite. As the particle size decreases from $\sigma^*_P=7$ to $\sigma^*_P=1$, particles move from the interface toward being uniform throughout both block copolymer microdomains. Both particle dispersion and particle-polymer interfacial structure are highly sensitive to the ratio of the particle diameter to the lamellar thickness.[119]

At low particle concentrations, the distribution of nanoparticles within the polymer matrix can be conveniently described by the difference in the insertion free energies at the lamellar interface and at the microdomain center, given by[120]

$$\delta\beta W=\beta(W_{\text{interface}}-W_{\text{domain}}) \quad (10)$$

If $\delta\beta W<0$, the particle prefers the lamellar interface; while for $\delta\beta W>0$, the particle prefers the microdomain. The maximum/minimum values of $\delta\beta W$correspond to the conditions of strong localization, *i.e.*, aggregation of the particles at the microdomain or interface. Fig. 11 shows the distribution of nanoparticles in the lamellar structure of symmetric diblock copolymers.[120] The theoretical results indicate that large particles are more easily localized in different positions of the lamellar structure. As shown in Fig.11(b) for particle distribution in two block copolymer lamellae with different chain lengths ($N=100$ and $N=200$), the one-body potential exhibits a periodic oscillation. For small particles ($R<5\ \sigma_s$), $\delta\beta W$ is independent of chain length. In this case, the distribution of nanoparticles is mainly determined by the inhomogeneity of the polymer density at the interface. As the particle size increases, $\delta\beta W$ is strongly affected by the lamellar thickness, leading to the oscillatory structure. Fig. 11(c) compares $\delta\beta W$ for two lamellae with different packing fractions

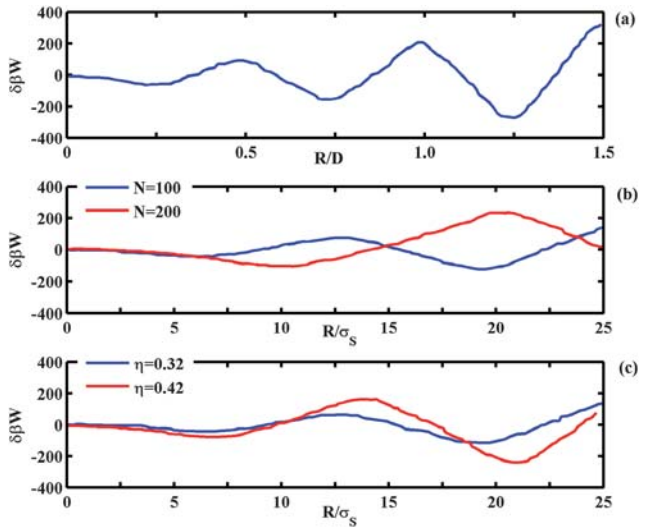

Fig. 11 The distribution of nanoparticles in the lamellar structures of symmetric diblock copolymers. (a) Dependence of $\delta\beta W$ on the particle radius to the lamellar periodic spacing (R/D). (b) Effect of the chain length on $\delta\beta W$. (c) Effect of the polymer density on $\delta\beta W$. Reprinted with permission from ref. 120.

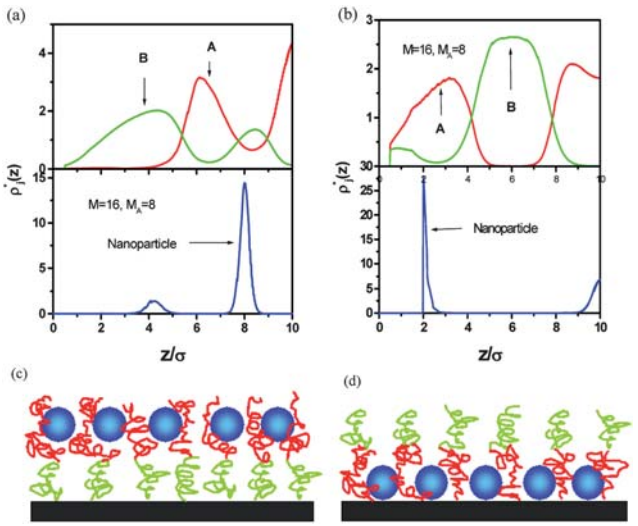

Fig. 12 Self-organization of nanoparticles in confined lamellae of symmetric block copolymers. (a) and (b): The reduced density profiles of polymeric segments and nanoparticles confined within the block copolymer thin film. (c) and (d): Visualizations of the hybrid materials corresponding to the density profiles given in (a) and (b), respectively. For (a) and (c), the "B" segments are neutral to the nanoparticles while for (b) and (d), the "B" segments are repelled to the particles. Reprinted with permission from ref. 123.

($\eta = 0.32$and $\eta = 0.42$). At different packing densities, the periodicities of the oscillation are dictated by their own lamellar periodic spacing. The DFT results show that nanoparticle distribution depends not only on the particle size and surface energy but also on the local structure of the microdomain interface, polymer chain length, as well as the polymer compressibility.[120]

4.3 Confinement effect

The properties of PNCs can be drastically influenced by the interactions of polymers and nanoparticles with a surface. Because of the entropic effect, polymer chains are depleted from a neutral surface, resulting in surface segregation of nanoparticles and even surface phase transition.[121] Confinement also complicates the mesoscopic phase behavior of block copolymers and nanoparticle self-organization within the polymer matrix.[122] To illustrate this subtle behavior, we show in Fig. 12 the microstructures for two binary mixtures of block copolymers and nanoparticles confined between two parallel neutral surfaces. While the block copolymers form a lamellar structure and the nanoparticles attract to one particular domain ("A" segments) of the block copolymer, the drastic difference in the morphologies, as depicted schematically by Fig. 12(c) and 12(d), is introduced by a small repulsion between the nanoparticles and the other block copolymer microdomain ("B" segments).[123] The dramatic response of PNC structure to particle-polymer interactions may be utilized for surface coating that prevents fouling by both hydrophobic and hydrophilic substances.

5. Summary and outlook

Polymer density functional theory (DFT) provides a promising computational tool to investigate the surface and interfacial behavior of polymers in an aqueous environment. In this article, we have reviewed applications of the DFT for exploring the antifouling properties of polymer brushes (PBs) and polymer nanocomposites (PNCs), by taking into account various important effects including the polymer architecture, excluded-volume, associating interactions, van der Waals forces, and Coulombic interactions. The numerical results show that the DFT predictions are in good agreement with experiments and molecular simulations for the polymer structure and surface properties. The theoretical calculations may help to relate the antifouling performance of polymeric materials to their chemical composition, molecular architecture, and surface properties. Such relation will find application in the rational design of new polymeric systems with improved antifouling performance.

We have demonstrated that the DFT is capable of describing polymer-mediated interactions, self-organization of nanoparticles, and the surface-induced behavior of polymer nanocomposites. It can also be used to predict condensation and layering phase transitions of adsorbed species near brush surfaces and phase transitions in particle-block copolymer mixture. Whereas applications of the DFT are mostly discussed in the context of drastically simplified molecular models, the theoretical framework is equally applicable to realistic polymeric and biological systems. Toward that end, we need reliable experimental results for quantifications of the model parameters (*e.g.*, polymer solubility and conformation in aqueous environments) and for calibrations of the theoretical predictions (*e.g.*, microscopic structures of polymer brushes and nanocomposites, and the adhesion behavior of proteins or colloidal particles). The theoretical calculations will then provide quantitative predictions on the antifouling performance of a given polymer surface or for the design and fabrication of polymer surfaces with optimal efficiency. By capturing the important features of polymers and

biological substances, the coarse-grained models may be used as an efficient computational platform to understand generic features of surface forces against non-specific adsorptions.

Appendix: Some practical strategies for formulation of the excess Helmholtz energy functional of polymeric systems

The essential task in application of DFT is to formulate an analytical expression for the intrinsic Helmholtz energy of a nonideal system as a functional of the molecular density profiles. For convenience, the Helmholtz energy functional is often divided into an ideal part and an excess. While the ideal part is known exactly, only approximate expressions are available for the excess intrinsic Helmholtz energy of polymeric systems of practical concern.

The intrinsic Helmholtz energy of a polymeric system is often formulated by using semi-empirical approximations. Common methods include the local density approximation (LDA), the mean-field approximation (MFA), and the weighted density approximation (WDA). LDA assumes that the excess free energy depends only on the local density. The simple procedure requires only the knowledge of the bulk properties. It yields reasonable results if the density profile changes smoothly over the length scale comparable to the molecular size. MFA gives an excess free energy that depends only on the inter-particle potential and the average local density. Like the van der Waals equation of state, MFA ignores intermolecular correlations and gives only qualitative or semi-quantitative results. More quantitative representation of the excess Helmholtz energy functional is often accomplished by using various WDAs. This method was first introduced by Nordholm and co-workers[124] in applications of DFT for inhomogeneous simple fluids and was later extended to polymeric systems.[35,125] In its simplest form, the excess Helmholtz energy functional is given by

$$F^{ex}[\rho(\boldsymbol{r})] = \int d\mathbf{r}'\rho(\mathbf{r}')f(\bar{\rho}) \tag{A1}$$

where $f(\bar{\rho})$ stands for the Helmholtz free energy per polymer segment in a bulk state with average density $\bar{\rho}$. The bulk Helmholtz energy can be obtained from an equation of state (EOS) and the weighted density $\bar{\rho}$ is defined by the local segment density and the Heaviside function Θ

$$\bar{\rho}(r) = \frac{3}{4\pi\sigma^3}\int dr'\rho(r')\Theta(|\mathbf{r}-\mathbf{r}'|-\sigma) \tag{A2}$$

The numerical performance of WDA depends on the bulk EOS and formulation of the weighted density.[36,39,126,127] WDA has been extensively used to study surface forces in polymeric fluids including systems containing flexible polymers,[36] semiflexible polymers,[128,129] star polymers,[114] and rods,[130] polymers with molecular weight polydispersity[131] as well as polymers of infinite length.[132]

In this appendix, we outline a generic procedure to account for the excess Helmholtz energy of polymer systems based on the intermolecular interactions, *i.e.*, in terms of the segment-level excluded-volume effect, intra-chain correlations and association, van der Waals attraction, and electrostatic forces. While each component of the intermolecular potential makes a distinct contribution to the excess free energy, the correlation effects are included by using various perturbation expansions and by solving the distribution of polymer segments self-consistently.

A.1 Excluded-volume effect

Originally developed by Rosenfeld for inhomogeneous hard-sphere fluids,[126,133] the fundamental-measure theory (FMT) is an elegant and powerful approach to account for short-range intermolecular interactions. A key idea behind FMT is to decouple the two-particle excluded-volume effects in terms of single-particle weighted densities, *i.e.*, four scalar- and two vector-weighted functions, $\{n_\alpha(\boldsymbol{r})|\alpha = 0,1,2,3,V1,V2\}$, that reflect the particle geometry. Unlike an empirically formulated weighted density in a typical WDA, FMT expresses the excess free energy in terms of the six weighted functions following a procedure similar to the classical scaling particle theory (SPT):

$$F_{hs}^{ex}[\rho(\boldsymbol{r})] = \int d\mathbf{r}'\phi_{hs}[n_\alpha(\boldsymbol{r}')]. \tag{A3}$$

Indeed, for bulk systems, the Helmholtz energy density ϕ_{hs} from FMT reproduces that from the Percus–Yevick (PY) approximation following the compressibility equation.[134] Further improvement of the FMT was proposed by Roth *et al.*[135] and independently by Yu *et al.*[136] In the modified FMT, the excess free energy functional is given by

$$\begin{aligned}\beta\phi_{hs} = &-n_0\ln(1-n_3) + \frac{n_1n_2 - \mathbf{n}_{V1}\cdot\mathbf{n}_{V2}}{1-n_3} \\ &+ \frac{1}{36\pi}\left[n_3\ln(1-n_3) + \frac{n_3}{(1-n_3)^2}\right]\frac{n_2 - 3n_2\mathbf{n}_{V2}\cdot\mathbf{n}_{V2}}{n_3}\end{aligned} \tag{A4}$$

The modified FMT uses the Boublik-Mansoori-Carnahan-Starling-Leland (BMCSL) EOS as the input and it improves the numerical performance, in particular, for highly asymmetric hard-sphere systems at high density. FMT has been extended to systems containing non-spherical particles.[137]

The main different between FMT and WDA is that FMT is formulated by interpolating the exact results at low density and macroscopic limits and is capable of *predicting* the structure and thermodynamic properties of bulk as well as inhomogeneous systems.[133] By contrast, a typical WDA *requires* the equation of state of the bulk fluid as an input. Besides, in FMT the Helmholtz energy functional is expressed in terms of multiple weighted densities and each weight function has clear geometric or physical significance. By contrast, a typical WDA uses only a single, often empirically selected weight function. In terms of the performance, FMT *predicts* not only accurate thermodynamic properties and one-body density profiles of inhomogeneous hard-sphere systems but also the pair and multi-body direct correlation function and bridge function of bulk fluids. On the other hand, WDA is formulated to *reproduce* the bulk direct correlation function.

Eqn (4) was incorporated by Yu and Wu[136,138] for polymeric fluids by combining the FMT for the short-ranged repulsion and the thermodynamic perturbation theory (TPT) for chain connectivity.[139] The FMT-based polymer DFT has been applied to various polymeric fluids, including flexible polymers,[138]

semiflexible polymers,[140] copolymers,[141,142] rods,[143,144] rod-coil,[41] polyeletrolytes,[103,145–147] tethered polymers,[76,103] and helical polymers[148] as well as polymers with complex architecture.[38,40,42] Recently, it was also extended to study the microstructure of polymers in two dimensional systems by employing a multi-scaled technique to solve the time-consuming problem.[148] It has been successfully used to investigate adsorption and surface phase transition,[149–151] the microstructure of flexible polymer fluids,[40,142,152] surface forces between polymer brushes[113,153] and physical properties of biological systems.[50,51]

A.2 Intra-chain correlation and association

The excess free energy due to intra-chain correlations accounts for the difference between the thermodynamic properties of a polymer system and those corresponding to a monomeric reference system of the same density profiles. This part of the excess free energy is often calculated from an extension of the thermodynamic perturbation theory (TPT) to inhomogeneous systems.[125] As proposed by Yu and Wu,[154] the free energy due to the intra-chain correlation can be expressed in terms of the weighted functions

$$F^{\mathrm{ex}}_{\mathrm{chain}} = (1-M)k_{\mathrm{B}}T\int \mathrm{d}\mathbf{r}' n_0 \zeta \ln y[n_\alpha(\mathbf{r}')] \tag{A5}$$

where $\zeta = 1-\boldsymbol{n}_{\mathrm{V2}}\cdot\boldsymbol{n}_{\mathrm{V2}}/n_2^2$, and y stands for the contact value of the local cavity correlation function of a uniform monatomic fluid. The excess free energy constructed in this manner should not be confused with the direct bonding potential considered in the ideal part of the free energy. As shown in eqn(A5), the intra-chain correlation depends only on the molecular architecture and interaction among monomeric segments. Yu and Wu suggested that the TPT method can be similarly extended to account for the thermodynamic nonideality due to formation of chemical or hydrogen bonds.[154]

Another approach to account for the chain connectivity and association is by using iSAFT, an extension of the SAFT equation of the state for inhomogeneous systems.[43–45] In this approach, the excess free energy incorporates both indirect intramolecular interactions and direct bonding interaction between neighboring segments. iSAFT can be easily applicable to polymers with complex architecture, such as branched polymers and dendrimers. It should be mentioned that most current versions of the polymer DFT deploy the first-order TPT (TPT1) to account for the intra-chain correlations. Because TPT1 is not accurate if the polymer bond length is very different from the segment diameter,[155] the polymeric molecules are often represented by freely-jointed tangent sphere chains. Besides, it is well known that TPT1 does not yield an accurate second virial coefficient and thus it is not reliable for semi-dilute systems.[109] For dilute polymer solutions and for systems containing branched or star polymers, a second order perturbation theory (TPT2) must be used in application of the polymer DFT.[156]

A.3 van der Waals attraction

The excess Helmholtz energy due to van der Waals attractions can be constructed by a second-order expansion of the excess free energy functional with respect to that of a uniform fluid[157]

$$\beta F^{\mathrm{ex}}_{\mathrm{att}} = \beta F_0(\rho_{\mathrm{b}}) + \beta\mu^{\mathrm{ex}}_{\mathrm{att}}\int \mathrm{d}\mathbf{r}[\rho(\mathbf{r})-\rho_{\mathrm{b}}] - \frac{1}{2}\int\int \mathrm{d}\mathbf{r}\mathrm{d}\mathbf{r}' c_b(|\mathbf{r}-\mathbf{r}'|)[\rho(\mathbf{r})-\rho_{\mathrm{b}}][\rho(\mathbf{r}')-\rho_{\mathrm{b}}] \tag{A6}$$

where F_0 stands for the excess free energy due to van der Waals attraction in the bulk fluid, $\mu^{\mathrm{ex}}_{\mathrm{att}}$ is corresponding the excess chemical potential, and $c_b(r)$ is the direct correlation function (DCF) of the bulk fluid. Like MFA, eqn(A6) is computationally very efficient, in particular when there is an analytical expression for the DCF of the bulk fluid.

A.4 Electrostatic interactions

Li and Wu[147] proposed that the excess Helmholtz energy due to electrostatic interactions can be described by a quadratic density expansion of the free energy functional with respect to that for a bulk fluid.[30,147,158] It was shown that the DFT faithfully accounts for both short- and long-ranged correlations of polyelectrolyte solutions. Specifically, the excess free energy due to the electrostatic interactions is given by

$$\begin{aligned}\beta F^{\mathrm{ex}}_{\mathrm{cl}} &= \tfrac{l_{\mathrm{B}}}{2}\sum_{i,j}\int\int \mathrm{d}\mathbf{r}\mathrm{d}\mathbf{r}'\frac{z_i z_j \rho_i(\mathbf{r})\rho_j(\mathbf{r}')}{|\mathbf{r}-\mathbf{r}'|} \\ &+\beta F_0\left(\{\rho_i^{\mathrm{b}}\}\right) - \sum_i \int \mathrm{d}\mathbf{r} c_i^{(1)}\left[\rho_i(\mathbf{r})-\rho_i^b\right] \\ &-\frac{1}{2}\sum_{i,j}\int\int \mathrm{d}\mathbf{r}\mathrm{d}\mathbf{r}' c_i^{(2)}\left[\rho_i(\mathbf{r})-\rho_i^{\mathrm{b}}\right]\left[\rho_i(\mathbf{r})-\rho_i^{\mathrm{b}}\right]\end{aligned} \tag{A7}$$

where ρ_i is the density profiles of molecule i (a polyion segment or a small ion), ρ_i^{b} is the bulk density, l_{B} is the Bjerrum length, and z_i is the particle valence. The electrostatic parts of the one-body and two-body DCFs, $c_i^{(1)}$ and $c_i^{(2)}$, are obtained from the mean-spherical approximation (MSA).[159] Eqn(A7) accounts for the direct Coulomb as well as the ionic correlations. In other words, the DFT is different from the Poisson–Boltzmann equation even without the ionic size effects. Application of the MSA equations to simple electrolyte solutions is well established.[160] At low ionic concentration, MSA reduces to the Debye–Hückel results.

In summary, this appendix outlines a generic procedure to formulate the free energy functional for model polymeric systems. As discussed in main text, alternative methods can also be used that yield comparable results. While we are mainly concerned with the qualitative behavior of polymers at interfaces and many important features can be captured by simple analytical methods (*e.g.*, the scaling analysis for the brush thickness), the advantage of the DFT method lies in its versatility and generality: a unified theoretical framework can be used to address a wide variety of different phenomena including those related to the solvent effects. Whereas simple formulations of the DFT (*e.g.*, local density and mean-field approximations) will often be sufficient for qualitative purposes, many interesting phenomena of polymers and polyelectrolytes in an aqueous environment are directly related to the local and long-range correlations that cannot be captured by simple methods.

Acknowledgements

This work is supported by the NSF of China (20776005, 20736002 and 20874005), Beijing Novel Program (2006B17), NCET Program (NCET-06-0095), ROCS Foundation (LX2007-02), and Novel Team (IRT0807) from the MOE of China, Chemical Grid Program from BUCT. Wu acknowledges the financial supports from the US National Science Foundation (CBET-0852353), the Department of Energy (DE-FG02-06ER46296), and National Institute of Health (R21AI077532-02).

References

1 D. G. Castner and B. D. Ratner, *Surf. Sci.*, 2002, **500**, 28.
2 S. Krishnan, C. J. Weinman and C. K. Ober, *J. Mater. Chem.*, 2008, **18**, 3405.
3 H. C. Flemming, *Appl. Microbiol. Biotechnol.*, 2002, **59**, 629.
4 D. Klee and H. Hocker, *Biomedical Applications: Polymer Blends*, 1999, **149**, 1.
5 M. R. Nejadnik, H. C. van der Mei, W. Norde and H. J. Busscher, *Biomaterials*, 2008, **29**, 4117.
6 V. Sambhy, M. M. MacBride, B. R. Peterson and A. Sen, *J. Am. Chem. Soc.*, 2006, **128**, 9798.
7 C. Bressy and A. Margaillan, *Prog. Org. Coat.*, 2009, **66**, 400.
8 K. C. Khulbe, C. Feng and T. Matsuura, *J. Appl. Polym. Sci.*, 2010, **115**, 855.
9 C. M. Grozea and G. C. Walker, *Soft Matter*, 2009, **5**, 4088.
10 D. M. Yebra, S. Kiil and K. Dam-Johansen, *Prog. Org. Coat.*, 2004, **50**, 75.
11 N. Fusetani, *Nat. Prod. Rep.*, 2004, **21**, 94.
12 A. S. Clare, *Biofouling*, 1996, **9**, 211.
13 G. G. Geesey, Z. Lewandowski, and H.-C. Flemming, '*Biofouling and biocorrosion in industrial water systems*', Lewis Publishers, 1994.
14 M. Fletcher, '*Bacterial adhesion: molecular and ecological diversity*', Wiley, 1996.
15 T. H. Bae, I. C. Kim and T. M. Tak, *J. Membr. Sci.*, 2006, **275**, 1.
16 P. Asuri, S. S. Karajanagi, R. S. Kane and J. S. Dordick, *Small*, 2007, **3**, 50.
17 M. P. Sun, Y. L. Su, C. X. Mu and Z. Y. Jiang, *Ind. Eng. Chem. Res.*, 2010, **49**, 790.
18 K. C. Anyaogu, A. V. Fedorov and D. C. Neckers, *Langmuir*, 2008, **24**, 4340.
19 W. M. de Vos, F. A. M. Leermakers, A. de Keizer, I. M. Kleijn and M. A. C. Stuart, *Macromolecules*, 2009, **42**, 5881.
20 P. G. de Gennes, '*Scaling concepts in polymer physics*', Cornell University Press, 1979.
21 G. H. Fredrickson, '*The equilibrium theory of inhomogeneous polymers*', Oxford University Press, 2006.
22 K. S. Schweizer and J. G. Curro, *Advances in Chemical Physics*, 1997, **98**, 1.
23 J. Z. Wu and Z. D. Li, *Annu. Rev. Phys. Chem.*, 2007, **58**, 85.
24 P. Hohenberg and W. Kohn, *Phys. Rev.*, 1964, **136**, B864.
25 N. D. Mermin, *Phys. Rev.*, 1965, **137**, 1441.
26 R. Evans, *Adv. Phys.*, 1979, **28**, 143.
27 R. G. Parr and W. Yang, '*Density-functional theory of atoms and molecules*', Oxford University Press, 1989.
28 R. Evans, in '*Density functionals in the theory of nonuniform fluids*', ed. D. Henderson, New York, 1992.
29 D. W. Oxtoby, *Annu. Rev. Mater. Res.*, 2002, **32**, 39.
30 J. Z. Wu, *AIChE J.*, 2006, **52**, 1169.
31 J. Z. Wu, in '*Density Functional Theory Tor Liquid Structure and Thermodynamics*', Berlin, 2009.
32 Y. X. Yu and J. Z. Wu, *J. Chem. Phys.*, 2003, **118**, 3835.
33 D. Chandler, J. D. McCoy and S. J. Singer, *J. Chem. Phys.*, 1986, **85**, 5977.
34 D. Chandler, J. D. McCoy and S. J. Singer, *J. Chem. Phys.*, 1986, **85**, 5971.
35 C. E. Woodward, *J. Chem. Phys.*, 1991, **94**, 3183.
36 C. E. Woodward and A. Yethiraj, *J. Chem. Phys.*, 1994, **100**, 3181.
37 C. E. Woodward and J. Forsman, *J. Chem. Phys.*, 2008, **129**, 054902.
38 X. F. Xu, D. P. Cao, X. R. Zhang and W. C. Wang, *Phys. Rev. E: Stat., Nonlinear, Soft Matter Phys.*, 2009, **79**, 021805.
39 A. Yethiraj and C. E. Woodward, *J. Chem. Phys.*, 1995, **102**, 5499.
40 D. P. Cao, T. Jiang and J. Z. Wu, *J. Chem. Phys.*, 2006, **124**, 164904.
41 L. S. Cheng and D. P. Cao, *J. Chem. Phys.*, 2008, **128**, 074902.
42 L. S. Cheng and D. P. Cao, *J. Phys. Chem. B*, 2007, **111**, 10775.
43 S. Tripathi and W. G. Chapman, *Phys. Rev. Lett.*, 2005, **94**, 087801.
44 S. Tripathi and W. G. Chapman, *J. Chem. Phys.*, 2005, **122**, 094506.
45 S. Jain, A. Dominik and W. G. Chapman, *J. Chem. Phys.*, 2007, **127**, 244904.
46 W. G. Chapman, G. Jackson and K. E. Gubbins, *Mol. Phys.*, 1988, **65**, 1057.
47 G. Jackson, W. G. Chapman and K. E. Gubbins, *Mol. Phys.*, 1988, **65**, 1.
48 J. P. Hansen and I. R. McDonald, '*Theory of simple liquids*', Academic Press, 1990.
49 D. Leckband and J. Israelachvili, *Q. Rev. Biophys.*, 2001, **34**, 105.
50 T. Jiang, Z. G. Wang and J. Z. Wu, *Biophys. J.*, 2009, **96**, 3065.
51 Z. D. Li, J. Z. Wu and Z. G. Wang, *Biophys. J.*, 2008, **94**, 737.
52 P. G. Degennes, *Macromolecules*, 1980, **13**, 1069.
53 S. T. Milner, T. A. Witten and M. E. Cates, *Macromolecules*, 1988, **21**, 2610.
54 T. Cosgrove, T. Heath, B. Vanlent, F. Leermakers and J. Scheutjens, *Macromolecules*, 1987, **20**, 1692.
55 S. C. Kim, S. H. Suh and B. S. Seong, *J. Chem. Phys.*, 2007, **127**, 114903.
56 T. Cosgrove, T. G. Heath, K. Ryan and T. L. Crowley, *Macromolecules*, 1987, **20**, 2879.
57 J. C. Marshall, T. Cosgrove, F. Leermakers, T. M. Obey and C. A. Dreiss, *Langmuir*, 2004, **20**, 4480.
58 M. Murat and G. S. Grest, *Macromolecules*, 1989, **22**, 4054.
59 K. Binder, *Eur. Phys. J. E*, 2002, **9**, 293.
60 J. U. Kim and M. W. Matsen, *Macromolecules*, 2008, **41**, 246.
61 P. G. de Gennes, *Adv. Colloid Interface Sci.*, 1987, **27**, 189.
62 I. Szleifer, *Biophys. J.*, 1997, **72**, 595.
63 B. M. Steels, J. Koska and C. A. Haynes, *J. Chromatogr., B: Biomed. Sci. Appl.*, 2000, **743**, 41.
64 D. Trombly and V. Ganesan, *J. Polym. Sci., Part B: Polym. Phys.*, 2009, **47**, 2566.
65 H. J. Taunton, C. Toprakcioglu, L. J. Fetters and J. Klein, *Nature*, 1988, **332**, 712.
66 T. Drobek, N. D. Spencer and M. Heuberger, *Macromolecules*, 2005, **38**, 5254.
67 F. Fang and I. Szleifer, *Langmuir*, 2002, **18**, 5497.
68 P. M. Konig, R. Roth and K. R. Mecke, *Phys. Rev. Lett.*, 2004, **93**, Art. No. 160601.
69 J. Satulovsky, M. A. Carignano and I. Szleifer, *Proc. Natl. Acad. Sci. U. S. A.*, 2000, **97**, 9037.
70 M. Borowko, W. Rzysko, S. Sokalowski and T. Staszewski, *J. Phys. Chem. B*, 2009, **113**, 4763.
71 M. Borowko, W. Rzysko, S. Sokolowski and T. Staszewski, *J. Chem. Phys.*, 2007, **126**, 214703.
72 J. F. Hester, P. Banerjee, Y. Y. Won, A. Akthakul, M. H. Acar and A. M. Mayes, *Macromolecules*, 2002, **35**, 7652.
73 S. Krishnan, R. Ayothi, A. Hexemer, J. A. Finlay, K. E. Sohn, R. Perry, C. K. Ober, E. J. Kramer, M. E. Callow, J. A. Callow and D. A. Fischer, *Langmuir*, 2006, **22**, 5075.
74 R. Sheparovych, M. Motornov and S. Minko, *Langmuir*, 2008, **24**, 13828.
75 J. Valle, S. Da Re, N. Henry, T. Fontaine, D. Balestrino, P. Latour-Lambert and J. M. Ghigo, *Proc. Natl. Acad. Sci. U. S. A.*, 2006, **103**, 12558.
76 X. F. Xu and D. P. Cao, *J. Chem. Phys.*, 2009, **130**, 164901.
77 M. Muller and L. G. MacDowell, *Europhys. Lett.*, 2001, **55**, 221.
78 O. Pizio, A. Patrykiejew and S. Sokolowski, *J. Phys. Chem. C*, 2007, **111**, 15743.
79 L. Zhou and Y. Q. Ma, *J. Phys.: Condens. Matter*, 2008, **20**, 095006.
80 S. Jain, V. V. Ginzburg, P. Jog, J. Weinhold, R. Srivastava and W. G. Chapman, *J. Chem. Phys.*, 2009, **131**, 044908.
81 S. A. Egorov, *J. Chem. Phys.*, 2008, **129**, 064901.
82 G. Kritikos and A. F. Terzis, *Polymer*, 2008, **49**, 3601.
83 T. M. Birshtein, P. A. Lakovlev, V. M. Arnoskov, F. A. M. Leermakers, E. B. Zhulina and O. V. Borisov, *Macromolecules*, 2008, **41**, 478.
84 D. I. Dimitrov, A. Milchev, K. Binder and D. W. Heermann, *Macromol. Theory Simul.*, 2006, **15**, 573.

85 E. B. Zhulina, T. M. Birshtein and O. V. Borisov, *Eur. Phys. J. E*, 2006, **20**, 243.
86 M. Ballauff and O. Borisov, *Curr. Opin. Colloid Interface Sci.*, 2006, **11**, 316.
87 M. Manghi, M. Aubouy, C. Gay and C. Ligoure, *Eur. Phys. J. E*, 2001, **5**, 519.
88 A. L. Frischknecht, *J. Chem. Phys.*, 2008, **128**, 224902.
89 N. Patel and S. A. Egorov, *J. Am. Chem. Soc.*, 2005, **127**, 14124.
90 D. J. Dyer, *Adv. Funct. Mater.*, 2003, **13**, 667.
91 B. D. Gates, Q. B. Xu, M. Stewart, D. Ryan, C. G. Willson and G. M. Whitesides, *Chem. Rev.*, 2005, **105**, 1171.
92 L. Ionov, V. Bocharova and S. Diez, *Soft Matter*, 2009, **5**, 67.
93 S. K. Nath, P. F. Nealey and J. J. de Pablo, *J. Chem. Phys.*, 1999, **110**, 7483.
94 C. Seok, K. F. Freed and I. Szleifer, *J. Chem. Phys.*, 2000, **112**, 6443.
95 C. Seok, K. F. Freed and I. Szleifer, *J. Chem. Phys.*, 2000, **112**, 6452.
96 H. Y. Chen, Z. C. Ye, C. J. Peng, H. L. Liu and Y. Hu, *J. Chem. Phys.*, 2006, **125**, 204708.
97 Y. Tran, P. Auroy, L. T. Lee and M. Stamm, *Phys. Rev. E: Stat. Phys., Plasmas, Fluids, Relat. Interdiscip. Top.*, 1999, **60**, 6984.
98 P. Pincus, *Macromolecules*, 1991, **24**, 2912.
99 T. Jiang, Z. D. Li and J. Z. Wu, *Macromolecules*, 2007, **40**, 334.
100 T. Jiang and J. Z. Wu, *J. Chem. Phys.*, 2008, **129**, 084903.
101 T. Jiang and J. Z. Wu, *J. Phys. Chem. B*, 2008, **112**, 7713.
102 R. Ni, D. P. Cao, W. C. Wang and A. Jusufi, *Macromolecules*, 2008, **41**, 5477.
103 T. Jiang, Z. D. Li and J. Z. Wu, *Macromolecules*, 2007, **40**, 334.
104 S. Block and C. A. Helm, *J. Phys. Chem. B*, 2008, **112**, 9318.
105 L. A. Utracki, M. Sepehr and E. Boccaleri, *Polym. Adv. Technol.*, 2007, **18**, 1.
106 R. Nigmatullin, F. Gao and V. Konovalova, *J. Mater. Sci.*, 2008, **43**, 5728.
107 H. Sawada, *Prog. Polym. Sci.*, 2007, **32**, 509.
108 R. Shenhar, T. B. Norsten and V. M. Rotello, *Adv. Mater.*, 2005, **17**, 657.
109 Z. D. Li and J. Z. Wu, *J. Chem. Phys.*, 2007, **126**, 144904.
110 J. Forsman and C. E. Woodward, *J. Chem. Phys.*, 2009, **131**, 044903.
111 E. Eiser, J. Klein, T. A. Witten and L. J. Fetters, *Phys. Rev. Lett.*, 1999, **82**, 5076.
112 E. Zhulina, C. Singh and A. C. Balazs, *Langmuir*, 1999, **15**, 3935.
113 D. P. Cao and J. Z. Wu, *Langmuir*, 2006, **22**, 2712.
114 C. E. Woodward and J. Forsman, *Macromolecules*, 2004, **37**, 7034.
115 M. Turesson, J. Forsman and T. Akesson, *Phys. Rev. E: Stat., Nonlinear, Soft Matter Phys.*, 2007, **76**, 021801.
116 J. Forsman, C. E. Woodward and B. C. Freasier, *J. Chem. Phys.*, 2003, **118**, 7672.
117 P. Bryk and S. Sokolowski, *J. Chem. Phys.*, 2004, **120**, 8299.
118 C. E. Woodward and J. Forsman, *Macromolecules*, 2009, **42**, 7563.
119 J. Z. Jin, J. Z. Wu and A. L. Frischknecht, *Macromolecules*, 2009, **42**, 7537.
120 J. H. Jin and J. Z. Wu, *J. Chem. Phys.*, 2008, **128**, 074901.
121 E. S. McGarrity, A. L. Frischknecht and M. E. Mackay, *J. Chem. Phys.*, 2008, **128**, 154904.
122 Q. Wang, *Journal of Chemical Physics*, 2007, 126.
123 D. P. Cao and J. Z. Wu, *J. Chem. Phys.*, 2007, **126**, 144912.
124 S. Nordholm, M. Johnson and B. C. Freasier, *Australian Journal of Chemistry*, 1980, **33**, 2139.
125 E. Kierlik and M. L. Rosinberg, *J. Chem. Phys.*, 1994, **100**, 1716.
126 P. Tarazona, J. A. Cuesta and Y. Martinez-Raton, *Lect. Notes Phys.*, 2008, **753**, 247.
127 A. Yethiraj, *J. Chem. Phys.*, 1998, **109**, 3269.
128 J. Forsman and C. E. Woodward, *J. Chem. Phys.*, 2003, **119**, 1889.
129 J. Forsman and C. E. Woodward, *Macromolecules*, 2006, **39**, 1261.
130 J. Forsman and C. E. Woodward, *Macromolecules*, 2006, **39**, 1269.
131 C. E. Woodward and J. Forsman, *Phys. Rev. Lett.*, 2008, **100**, 098301.
132 C. E. Woodward and J. Forsman, *Phys. Rev. E: Stat., Nonlinear, Soft Matter Phys.*, 2006, **74**, 010801.
133 R. Roth, *J. Phys.: Condens. Matter*, 2010, **22**, 063102.
134 Y. Rosenfeld, *Phys. Rev. Lett.*, 1989, **63**, 980.
135 R. Roth, R. Evans, A. Lang and G. Kahl, *J. Phys.: Condens. Matter*, 2002, **14**, 12063.
136 Y. X. Yu and J. Z. Wu, *J. Chem. Phys.*, 2002, **117**, 10156.
137 H. Hansen-Goos and K. Mecke, *Phys. Rev. Lett.*, 2009, **102**, 018302.
138 Y. X. Yu and J. Z. Wu, *J. Chem. Phys.*, 2002, **117**, 2368.
139 M. S. Wertheim, *J. Chem. Phys.*, 1987, **87**, 7323.
140 D. P. Cao and J. Z. Wu, *J. Chem. Phys.*, 2004, **121**, 4210.
141 D. P. Cao and J. Z. Wu, *J. Chem. Phys.*, 2005, **122**, 194703.
142 D. P. Cao and J. Z. Wu, *Macromolecules*, 2005, **38**, 971.
143 D. P. Cao, L. S. Cheng and W. C. Wang, *Chin. Phys.*, 2007, **16**, 2296.
144 X. F. Xu, D. P. Cao and W. C. Wang, *J. Phys.: Condens. Matter*, 2008, **20**, 425221.
145 T. Jiang and J. Z. Wu, *J. Chem. Phys.*, 2008, **129**, 084903.
146 Z. D. Li and J. Z. Wu, *J. Phys. Chem. B*, 2006, **110**, 7473.
147 Z. D. Li and J. Z. Wu, *Phys. Rev. Lett.*, 2006, **96**, 048302.
148 X. F. Xu and D. P. Cao, *J. Chem. Phys.*, 2009, **131**, 054901.
149 P. Bryk, O. Pizio and S. Sokolowski, *J. Chem. Phys.*, 2005, **122**, 194904.
150 P. Bryk and S. Sokolowski, *J. Chem. Phys.*, 2004, **121**, 11314.
151 P. Bryk, K. Bucior, S. Sokolowski and G. Zukocinski, *J. Phys. Chem. B*, 2005, **109**, 2977.
152 D. P. Cao, M. H. Zhu and W. C. Wang, *J. Phys. Chem. B*, 2006, **110**, 21882.
153 D. P. Cao and J. Z. Wu, *Langmuir*, 2005, **21**, 9786.
154 Y. X. Yu and J. Z. Wu, *J. Chem. Phys.*, 2002, **116**, 7094.
155 Y. Zhou and G. Stell, *J. Chem. Phys.*, 1992, **96**, 1504.
156 A. Malijevsky, P. Bryk and S. Sokolowski, *Phys. Rev. E: Stat., Nonlinear, Soft Matter Phys.*, 2005, **72**, 032801.
157 Y. P. Tang and J. Z. Wu, *Phys. Rev. E: Stat., Nonlinear, Soft Matter Phys.*, 2004, **70**, 011201.
158 C. N. Patra, R. Chang and A. Yethiraj, *J. Phys. Chem. B*, 2004, **108**, 9126.
159 L. Blum, *Mol. Phys.*, 1975, **30**, 1529.
160 J. P. Simonin, L. Blum and P. Turq, *J. Phys. Chem.*, 1996, **100**, 7704.
161 A. N. Semenov, *Macromolecules*, 1992, **25**, 4967.

